Scientia Iranica C (2023) 30(6), 2001–2010

Sharif University of Technology
Scientia Iranica
Transactions C: Chemistry and Chemical Engineering
http://scientiairanica.sharif.edu

The first study of adsorption of methylene blue by Black Titania (B-TiO_2) nanoparticle in aqueous solution

M. Soleimani, E. Boorboor Azimi, M. Mousavi, J.B. Ghasemi, and A. Badiei*

School of Chemistry, College of Science, University of Tehran, Tehran, Iran.

Received 30 July 2021; received in revised form 9 November 2021; accepted 17 October 2022

KEYWORDS
Black titania;
Nanoparticle;
Methylene blue;
Adsorption isotherm;
Kinetic studies.

Abstract. This study investigates the elimination of Methylene Blue (MB) by adsorption on Black Titania (B-TiO_2) in an aqueous solution in the dark room. B-TiO_2 was prepared via the reduction of white TiO_2 by $NaBH_4$ in a tube furnace under an inert gas atmosphere at 600°C. Characterization of the absorbent was carried out by X-Ray Diffraction (XRD), N_2 adsorption-desorption, Scanning Electron Microscopy (SEM) mapping, photoluminescence, Energy Dispersive X-ray spectrometry (EDX) analysis, Zeta potential, Dynamic Light Scattering (DLS), and Fourier Transform Infrared Spectrometer (FT-IR). The maximum adsorption capacity of B-TiO_2 was found to be 88.65 mg g^{-1}. The rate-limiting step was the intra-particle diffusion stage. Maximum adsorption was observed under the following conditions: 26 mg of B-TiO_2 at pH 6 and MB concentration of 10 mg L^{-1}. It was demonstrated that B-TiO_2 might be recycled six times with very good adsorption results while keeping its high removal efficiency.

1. Introduction

The use of coloring agents and dyestuff is indispensable in today's paper, plastic, food, and cosmetics industries. The extensive use of these materials points to their substantial effect on different aspects of the environment, e.g., increase in Chemical Oxygen Demand (COD) of water bodies and adsorption of some of the sunlight entering water systems. They also exert adverse effects on aquatic ecosystems [1–3]. Following the aggravation of the environmental problems, severe problems ensue, e.g., presence of dyestuff in sewage waters and subsequently, lack of treatment methods. One efficient and advantageous option is use of adsorbents. Adsorption is a non-complicated and straightforward process for the purposes of design and use. More importantly, it is insensitive to toxic chemicals [4]. To investigate the properties and the effect of several adsorbent materials, the most commonly used dyestuffs that attract the most attention were methyl orange, Methylene Blue (MB), and Rhodamine B [5–8]. MB exists in many diverse materials including rubbers, pharmaceuticals, pesticides, varnishes, etc. as coloring agents and disinfectors. Graphene was proposed for MB adsorption [9]. The magnetic composite bio-sorbent could absorb MB with a capacity of 95 mg g^{-1} and recover four times [10]. The stronger capability to absorb MB was observed in organo-bentonite [11]. It was also concluded that grafted cyclodextrin-chitosan with multiple functional groups could be a good candidate

*. *Corresponding author.*
E-mail addresses: soleimanide@yahoo.de (M. Soleimani); eazimi.1989@gmail.com (E. Boorboor Azimi); mitra3954@yahoo.com (M. Mousavi); jahan.ghasemi@ut.ac.ir (J.B. Ghasemi); abadiei@ut.ac.ir (A. Badiei)

doi: 10.24200/sci.2022.58793.5897

for MB adsorption [12]. The ability of activated carbon to absorb MB, bromophenol blue, alizarine red-S, eriochrome black-T, malachite green, phenol red, and methyl violet from aqueous media was examined [13]. The elimination of MB with sulfonate-functionalized nano-porous silica spheres [14] and the removal of MB with jute fiber carbon [15], carbon-doped graphitic carbon nitride [16], activated carbons [17], graphitic carbon nitride doped with the S-block metals [18], mesoporous carbon nitride [19], barium phosphate nano-flake [20], titania/gum tragacanth nanohydrogel [21], binary TiO_2/reduced graphene oxide nanocomposite [22,23], diphenylanthrazoline compounds [24], soluble graphene nanosheets [25], graphene oxide/WO_3 nanorod composites [26], graphene oxide modified with Fe_3O_4 nanoparticles [27], CdS nanostructures [28], and porous graphene wrapped $SrTiO_3$ nanocomposite [29] have been introduced earlier.

Hydrogenation changes the important properties of nano TiO_2. The synthesis of hydrogenated titanium dioxide (Black Titania, B-TiO_2) was performed by extending optical adsorption to the infrared region [30]. Increase in the absorption results from the introduction of the mid-gap energy level in B-TiO_2 above the valance band caused by the wide-spreading overlap of O and Ti orbitals associated with the hybridization of H orbitals with S orbitals of titanium in TiO_2 samples (Scheme 1). These improved properties have led to an increase in the scope of research done on B-TiO_2 nanomaterials. Due to their properties, B-TiO_2 nanomaterials have been applied to various fields, e.g., photocatalysis, Lithium-Ion Batteries (LIM), supercapacitor, fuel cell, field emission, and microwave adsorption and photothermal therapy of cancer. B-TiO_2 is a complex composition of Ti^{4+} and Ti^{3+}, which is generally employed as a potential photocatalyst. During these photocatalytic reactions, we noticed its high adsorption properties. The adsorption property of B-TiO_2 and its photocatalytic property are quite attractive and they can expand the range of performances and applications as well as effectiveness of B-TiO_2. Therefore, this study investigates the adsorption properties of B-TiO_2.

Our goal is to eliminate MB dye from water by studying and providing adsorption performance of B-TiO_2 in the dark room to avoid photocatalytic reactions (B-TiO_2). First, B-TiO_2 is prepared and then, the effects of crucial variables including the concentration of MB dye and time are investigated (at optimized adsorbent dosage and pH). Adsorption kinetics and isotherms are analyzed separately using various models and the possible mechanisms for MB adsorption on to B-TiO_2 are discussed.

2. Experimental

The following models of instruments were used for the characterization of the nanomaterials. A Philips Xpert X-ray diffractometer was applied to prepare the X-Ray Diffraction (XRD) patterns. Fourier Transform Infrared Spectrometer (FT-IR) spectra were recorded on a WQF-510A FT-IR spectrophotometer. LEO 1430VP SEM-EDX instrument operation was applied in the Energy Dispersive X-ray Spectrometry (EDS) mode. An FEI NANOSEM 450 FESEM was used for the investigation of the morphologies of the adsorbent. JEOL JEM- 2100F provided Transmission Electron Microscopy (TEM) and High Resolution Transmission Electron Microscopy (HRTEM) images, which were exploited to gather more information about microstructure. A UV-Vis spectrophotometer (Scinco 4100) was utilized to observe the UV-visible. Agilent G9800A Luminescence Spectrometer extracted the photoluminescence results.

2.1. Preparation of B-TiO_2

The used procedure is as follows: 1.50 g of anatase TiO_2 nanoparticles were mixed with 0.71 g of $NaBH_4$ powder (the molar ratio between TiO_2 and $NaBH_4$ is 1:1). The resulting powder was homogenized and calcinated at 600°C in a tube furnace under argon gas

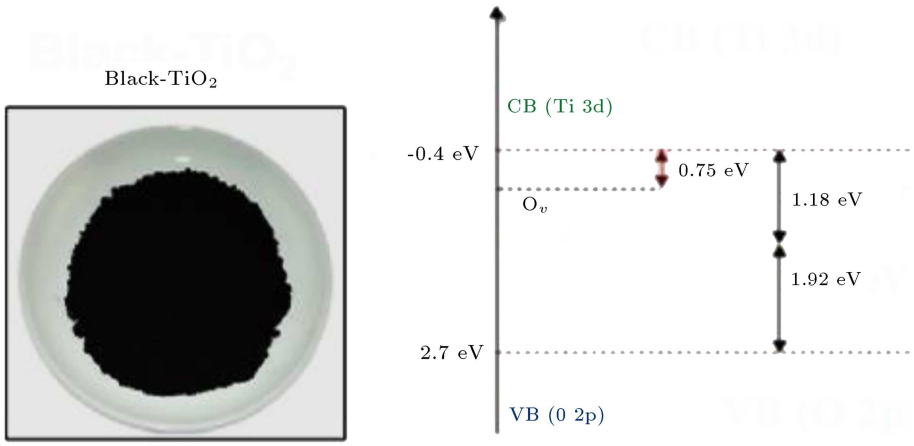

Scheme 1. Energy levels and band gaps of B-TiO_2.

for 30 minutes and then, cooled slowly under the same atmosphere for 5 hours. In the last section, B-TiO_2 was washed with ethanol and distilled water.

3. Characterization of the adsorbent (B-TiO_2)

X-ray diffraction patterns were utilized to analyze the crystal phase and microstructure of B-TiO_2, as presented in Figure 1. There are four typical crystal peaks at 26.8°(1 0 1), 37.5°(0 0 4), 42.6°(2 0 0), and 62.3°(2 0 4) with the anatase TiO_2 (JCPDS No. 21-1272) as a possible form [31]. The crystallite size was calculated using Scherrer's formula:

$$D = K\lambda/\beta\cos\theta, \tag{1}$$

where D is the crystal size, K Scherrer's constant usually taken as (0.89), λ the X-ray wavelength of Cu Kα radiation (λ = 1.54056 Å), β Full Width at Half Maximum (FWHM) of the (1 0 1) peak in radians, and θ Bragg's diffraction angle. $D = (0.89 \times 1.54)/(0.9 \times 2\pi/360)\cos(26.7/2) = 9.02$ nm, which is inconsistent with the previous report [32]. Moreover, the specific surface area of the prepared B-TiO_2 nanoparticles was obtained using the formula below:

$$S = 6 \times 10^3/dD, \tag{2}$$

where d is the theoretical density particle (3.894 g/cm^3) and $S = 6^*10^3/(3.894^*9.02) = 170$ m^2g^{-1}. This calculated specific surface area from XRD data is compatible with SEM-EDX mapping of the prepared B-TiO_2, as shown in Figure 2. The SEM-EDX mapping method presented in Figure 2(a)–(d) was employed to evaluate the morphological properties of B-TiO_2. Spherical B-TiO_2 nanoparticles with dark colors are also shown in Figure 2(a). In Figure 2(b)–(d), bright lattice fringes with 0.350 nm interplane distances are observed, which aptly conform to anatase B-TiO_2 (1 0 1) crystallographic planes [33]. The results of the Energy Dispersive X-ray spectrometry (EDX) analysis verify that elemental compositions remain unchanged in comparison with starting materials. The unambiguous distributions of Ti and O elements are further demonstrated by EDX elemental mappings of B-TiO_2 nanoparticles, which also show their homogenous distribution.

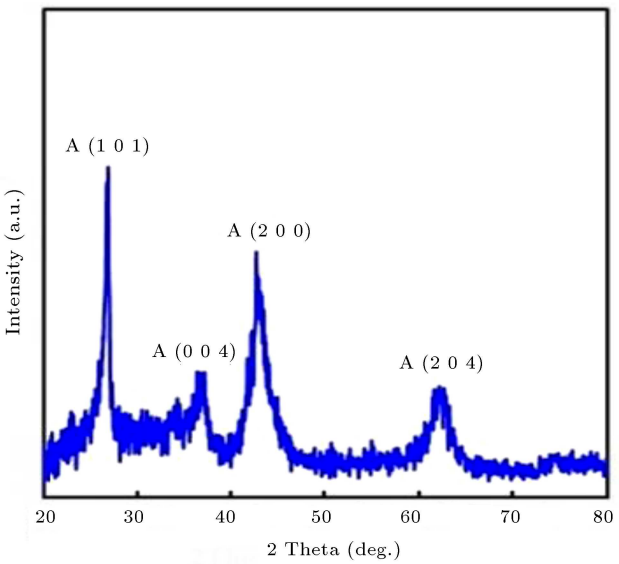

Figure 1. XRD pattern of B-TiO_2.

Charges on the surface of the B-TiO_2 sample were examined by Zeta potential analysis at pH = 7. As presented by Figure S1a (Supplementary data), B-TiO_2 has a zeta potential of +23.7 mV. A Dynamic Light Scattering (DLS) method was utilized to analyze the particle size distribution of B-TiO_2. An ultrasonic field was employed to disperse the samples in the form of powder and a suspension was made. The hydrodynamic diameter of the B-TiO_2 was measured to be around 38.2 nm (Figure S1b (Supplementary data)). The small size of these particles is enough to create a balanced suspension in deionized water. FT-IR spectroscopy is an effective technique to identify the functional groups. The FT-IR spectra of TiO_2 and B-TiO_2 samples are shown in Figure 3. For both samples, the broad peaks at 2805–3541 cm^{-1} correspond to the stretching vibration of the O-H surface-absorbed water molecules. The adsorption bands located at about 562 cm^{-1} are seen due to Ti-O vibration. Furthermore, the broad peak at 420–830 cm^{-1} is ascribed to the Ti-O-Ti [34].

Surface features, e.g., large surface area and high porosity of an adsorbent, can supposedly offer more active sites for efficient adsorption. On the basis of the classification of International Union of Pure and Applied Chemistry (IUPAC), the isotherm of the sample is the typical type IV with H3 hysteresis loop in the relative pressure range of 0.4–1.0 (p/p_0), indicating that it has mesoporous structure characteristics. The pore size distribution in the peak at 5 nm corresponds to the mesoporous structure. The interconnected porous network at interiors is also likely allowed. The formed network facilitates the interaction with more reactants which, in turn, will increase the adsorption ability. The N_2 adsorption-desorption isotherms of B-TiO_2 are shown in Figure 4. The surface area of B-TiO_2 is 166 m^2g^{-1}, the mean pore diameter 5.1 nm, and the total pore volume 0.242 cm^3 g^{-1}. This amount of porosity results from the sintering of nanoparticles at 600°C during B-TiO_2 preparation. The value of the specific surface area is determined by a Porosimeter as 166 m^2g^{-1}), which is almost consistent with the value calculated based on XRD data (170 m^2g^{-1}).

4. Adsorption isotherms study

Because of the large surface area, large pore volume,

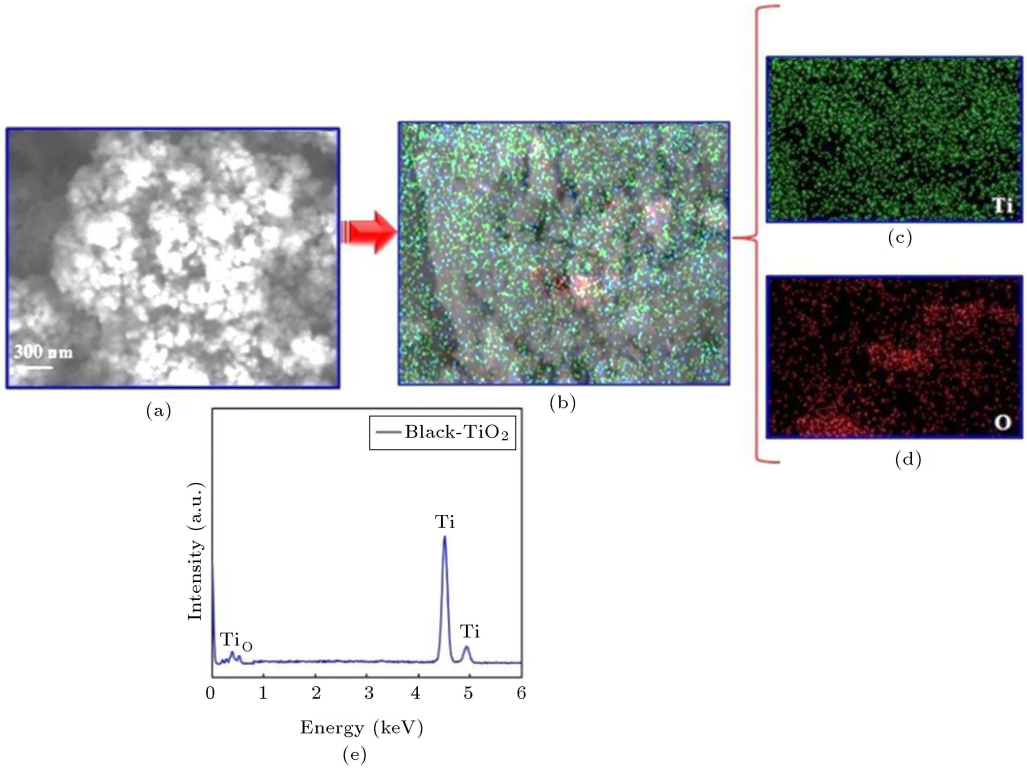

Figure 2. SEM-EDX mapping (a–d) and EDX analysis of B-TiO_2 (e).

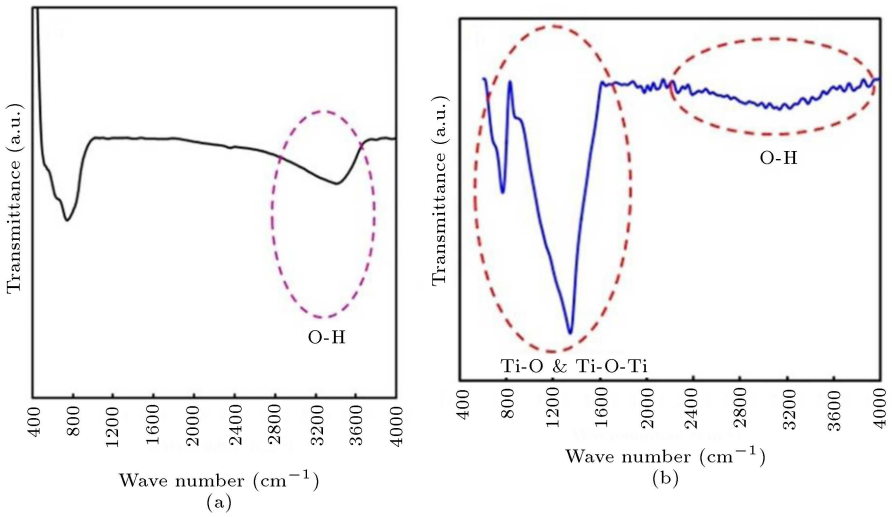

Figure 3. FT-IR spectra of TiO_2 (a) and B-TiO_2 (b).

and higher hydrothermal stability, the as-prepared B-TiO_2 has great potential for MB adsorption. Adsorption comprises a series of mass transfer phenomena. Conventionally, it means the sample adhesion to the surface of a liquid or a solid material (i.e., adsorbent). Isotherms of adsorption are the identifying factors that denominate the relations between adsorbent and adsorbates at a specific temperature in equilibrium. It is possible to find a proper model for the design process by properly conforming experimental data to various isotherm models. These models will produce instrumental parameters in obtaining essential data regarding the mechanism, surface features, and sorbent affinities [35]. The data collected from performed experiments have been fitted with some isotherm models to validate and examine their applicability. Table S1 (Supplementary data) shows the values of the coefficients obtained by these isotherm models. Q_m was approximated by investigating Langmuir's isotherm model [36]. A comprehensive monolayer exposure is thereby found on the sorbent's surface. The Langmuir's isotherm may be presented in a linear form

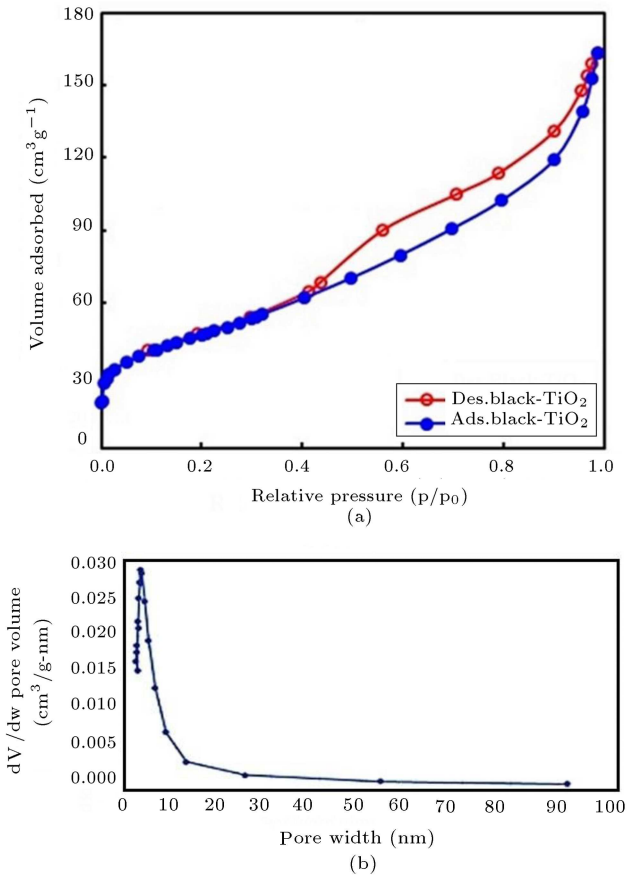

Figure 4. N_2 adsorption-desorption isotherm (a) and pore diameter distributions (b) of B-TiO_2.

as follows:

$$\frac{C_e}{q_e} = \frac{1}{K_a Q_m} + \frac{1}{Q_m} C_e, \tag{3}$$

where Q_m is the maximum adsorption capacity (mg g^{-1}) and K_a is the constant of adsorption equilibrium of Langmuir equation (Lmg^{-1}). According to Figure S2 (Supplementary data), unknown coefficients can be found with a plot of C_e/q_e against C_e. Freundlich's isotherm [37] is an experimental equation, which can identify heterogeneous structures and be presented in this way:

$$\ln(q_e) = \ln(K_F) + \frac{1}{n_F} \ln(C_e), \tag{4}$$

where K_F is Freundlich constant (L g^{-1}) of sorption and is correlated with bonding energy. It also represents the amount of dye absorbed on the adsorbent. n_F value indicates the degree of nonlinearity between dye concentration and adsorption. In the case of $n_F = 1$, the adsorption is linear and $n_F < 1$ indicates that the adsorption process is chemical. If it is greater than 1, physical adsorption is privileged [38].

As is shown in Table S1 (Supplementary data), n_F is greater than one, which means that the MB adsorption on B-TiO_2 is a physical process. Based on the above-presented results and R^2 values, it can be concluded that Langmuir's isotherm (monolayer adsorption on the homogeneous surface of sorbents) shows a better mechanism for the equilibrium of the adsorption process ($R^2 = 0.989$) than Freundlich's ($R^2 = 0.957$). In Temkin's isotherm equation, 'the heat of adsorption' is a factor that considers adsorption interactions. This equation is written as follows:

$$q_e = B_T \ln(A_T) + B_T \ln(C_e), \tag{5}$$

where $B_T = R_T/b_T$ and b_T correlates with the adsorption heat. A plot of q_e versus $\ln(C_e)$ was applied to estimate constants and coefficients of the linear isotherm (Figure S2 (Supplementary data); Table S1(Supplementary data)). It is concluded based on the examined data that since the correlation coefficient is not large enough (Figure S2 (Supplementary data)), Temkin's isotherm cannot be the right mechanism to explain the MB adsorption on to B-TiO_2.

The most appropriate model that fits the experimental data is Langmuir's isotherm, perhaps (Figure S3 (Supplementary data)). Temkin's model promptly changes into Langmuir's equation; however, if C_e approaches zero, Freundlich's isotherm is formed. Therefore, it is justified that greater adsorption be done physically.

5. Effect of contact time and initial dye concentration

Figure 5 displays the empirical results for MB adsorption on B-TiO_2 at different concentrations (60, 110, and 210 mg g^{-1}) concerning contact time. Although the dye concentration is inversely proportional

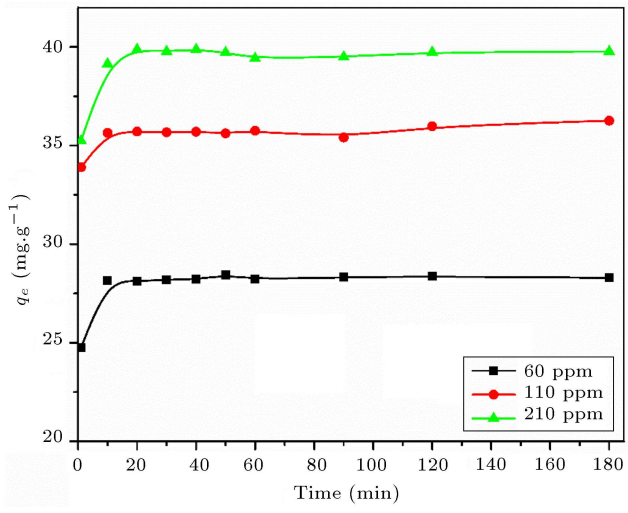

Figure 5. Effect of contact time and initial dye concentration on the adsorption capacity and MB adsorption (pH = 6, RT).

Table 1. Comparison between maximum adsorption capacities for MB for different adsorbents.

No.	Adsorbent	Q_m (mg g^{-1})	Time (min)	Reference
1	B-TiO_2	88.65	10	This work
2	Fiber carbon	225.64	75	[38]
3	C–C_3N_4-20	57.87	20	[39]
4	Natural zeolite	29.18	100	[40]
5	Chitosan modified zeolite	37.04	-	[41]
6	Active carbon	9.81	40	[42]
7	Apricot stones	36.68	80	[43]
8	Cherry sawdust	39.84	150	[44]
9	NSS-SO_3	208	60	[45]
10	MCN	360.8	50	[46]
11	Peat	324	40	[47]
12	SBA-15	280	60	[48]
13	Halloysite nanotubes	84.32	60	[49]
14	Mesoporous hybrid xerogel	144	120	[50]

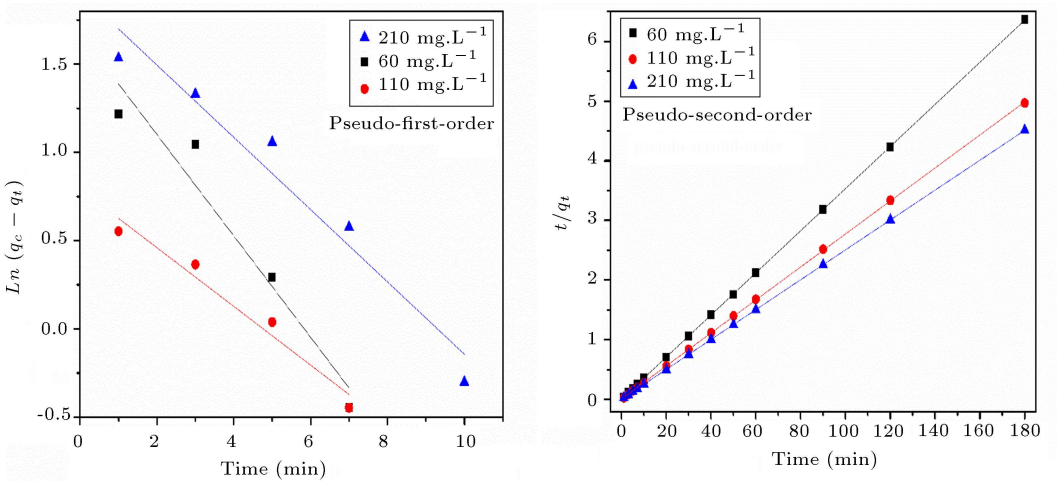

Figure 6. Plots of pseudo-first-order and pseudo-second-order, (pH = 6, RT).

to the adsorption percentage, the real amount of dye absorbed per unit mass of B-TiO_2 increases at higher concentrations. Following the rise of MB concentration from 60 to 210 mg g^{-1}, the adsorption capacity also increases from 28.14 to 39.14 mg g^{-1}. In all of the considered concentrations, the equilibrium was achieved in 10 minutes, being decidedly smaller than some other conventional adsorbents of MB. The results are illustrated in Table 1 [38–51]. It can be inferred from the single, continuous, and smooth curves leading to saturation shown in Figure 5 that a monolayer of MB may cover the surface of B-TiO_2.

6. Adsorption kinetic study

Having a deeper knowledge of how adsorption kinetics works in order to evaluate the mechanism of the reaction is quite necessary. It helps identify the best-operating conditions for adsorption. A few kinetic models were, therefore, employed for the MB adsorption kinetic study. The linear forms of pseudo-first-order and pseudo-second-order kinetic models are respectively described as follows:

$$\ln(q_e - q_t) = \ln(q_e) - k_1 \cdot t, \tag{6}$$

$$\frac{t}{q_t} = \frac{1}{k_2 q_e^2} + \frac{1}{q_e} t, \tag{7}$$

where k_1 (min^{-1}) and k_2 (g mg^{-1} min^{-1}) are the first- and second-order kinetic rate constants. The plots are shown in Figure 6 according to Eqs. (6) and (7). As seen in Table S2 (Supplementary data), the value of q_e determined by the pseudo-second-order reaction equation is close to the experimental one. This proves that the pseudo-second-order reaction equation

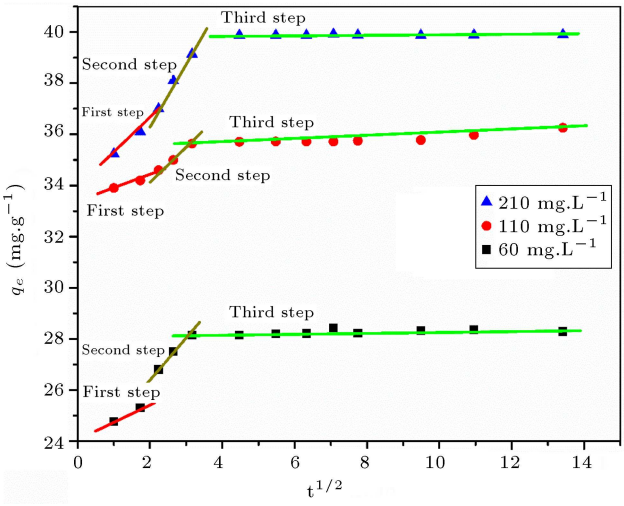

Figure 7. Intraparticle diffusion model for the MB adsorption on B-TiO_2, (pH = 6, RT).

is predominant. R^2 value, as another statistical indicator, is close to one, thus confirming the pseudo-second-order kinetic rate model. As indicated in a normal pseudo-second-order reaction, the adsorption process may be influenced by the amount of both MB and the adsorbent [52]. The intra-particle diffusion kinetic model was investigated to examine the rate-determining stage of the MB adsorption on B-TiO_2 as follows:

$$q_t = k_{dif} t^{1/2} + C, \tag{8}$$

where K_{dif} is the rate constant of the intra-particle diffusion model (mg $g^{-1}min^{-1/2}$) and C designates the width of the boundary layer. This model entails three steps: (1) adsorbate molecules penetrate the solid surface from the aqueous solution; (2) intra-particle diffusion occurs; and (3) the ultimate equilibrium is reached. Three linear regions, according to Eq. (8), are shown in Figure 6. This means that the adsorbent affects the dye adsorption through multiple procedures rather than only one procedure (Figure 7). As estimated from the second regression line (Table S2 (Supplementary data)), R^2 value is close to 1, which indicates that the applied model has verified the rate-limiting step as an intra-particle diffusion step.

7. Reusability study

Reusability is crucial, economically and environmentally, to the viability of an adsorbent. Therefore, the characteristic of 'reusability' was examined in the case of B-TiO_2 by the adsorption process of MB. The method included six adsorption-desorption cycles; the absorbed MB on B-TiO_2 was desorbed by washing with ethanol twice. In this regard, after each cycle, the B-TiO_2 was mixed with ethanol, centrifuged, and dried to be ready for the next adsorption cycle. Each cycle was repeated several times to compensate for the adsorbent weight loss. The whole cycle was repeated six times. There was no considerable decrease even after six cycles (Figure S4 (Supplementary data)). With such high reusability quality, B-TiO_2 can be considered a very good candidate for the adsorption of MB from industrial sewer waters.

8. Conclusion

Experiments on Black-Titania (B-TiO_2) for removing Methylene Blue (MB) from aqueous solutions in the dark room produced excellent results and the maximum adsorption capacity was achieved as 88.65 mg g^{-1}. After examining experimental data, the equilibrium isotherms were found to be significantly consistent with the Langmuir isotherm. The adsorption process was completed in just 10 minutes. The rate-determining stage in MB adsorption by B-TiO_2 may be the intra-particle diffusion stage. Washing with EtOH can quickly regenerate B-TiO_2, which can be reused multiple times to adsorb MB while keeping its efficiency relatively the same.

Acknowledgment

The authors acknowledge the National Elites Foundation of Iran and the University of Tehran for assisting this research financially.

Supplementary data

Supplementary data is available at:
http://scientiairanica.sharif.edu/jufile?ar_sfile=171059

References

1. Luo, P., Zhao, Y.F., Zhang, B., et al. "Study on the adsorption of Neutral Red from aqueous solution onto halloysite nanotubes", *Water Res.*, **44**, pp. 1489–1497 (2010).
2. Yan, H., Zhang, W.H., Kan, X.W., et al. "Sorption of methylene blue by carboxymethyl cellulose and reuse process in a secondary sorption", *Colloids Surf.*, **A 380**, pp. 143–151 (2011).
3. Saleh, T.A. and Gupta, V.K. "Photo-catalyzed degradation of hazardous dye methyl orange by use of a composite catalyst consisting of multi-walled carbon nanotubes and titanium dioxide", *J. Colloid Interface Sci.*, **371**, pp. 101–106 (2012).
4. El-Safty, S.A., Shahat, A., and Awual, M.R. "Efficient adsorbents of nanoporous aluminosilicate monoliths for organic dyes from aqueous solution", *J. Colloid Interface Sci.*, **359**, pp. 9–18 (2011).
5. Zhang, P., Qian, G.R., Shi, H.S., et al. "Mechanism of interaction of hydrocalumites (Ca/Al-LDH) with

methyl orange and acidic scarlet GR", *J. Colloid Interface Sci.*, **365**, pp. 110–116 (2012).

6. Jiang, R., Fu, Y.Q., Zhu, H.Y., et al. "Removal of methyl orange from aqueous solutions by magnetic maghemite/chitosan nanocomposite films: Adsorption kinetics and equilibrium", *J. Appl. Polym. Sci.*, **125**, pp. E540–E549 (2012).
7. Xie, G.Q., Xi, P.X., Liu, H.Y., et al. "A facile chemical method to produce superparamagnetic graphene oxide-Fe_3O_4 hybrid composite and its application in the removal of dyes from aqueous solution", *J. Mater. Chem.*, **22**, pp. 1033–1039 (2012).
8. Chi, Y., Geng, W.C., Zhao, L., et al. "Comprehensive study of mesoporous carbon functionalized with carboxylate groups and magnetic nanoparticles as a promising adsorbent", *J. Colloid Interface Sci.*, **369**, pp. 366–372 (2012).
9. Wu, T., Cai, X., Tan, S., et al. "Adsorption characteristics of acrylonitrile, p-toluenesulfonic acid, 1-naphthalenesulfonic acid and methyl blue on graphene in aqueous solutions", *Chem. Eng. J.*, **173**, pp. 144–149 (2011).
10. Fan, L.L., Luo, C.N., Li, X.J., et al. "Fabrication of novel magnetic chitosan grafted with graphene oxide to enhance adsorption properties for methyl blue", *Journal of Hazardous Materials.*, **215**(216), pp. 272–279 (2012).
11. Hao, X.L., Liu, H., Zhang, G.S., et al. "Magnetic field assisted adsorption of methyl blue onto organobentonite", *Appl. Clay Sci.*, **55**, pp. 177–180 (2012).
12. Fan, L.L., Zhang, Y., Luo, C.N., et al. "Synthesis and characterization of magnetic β-cyclodextrin-chitosan nanoparticles as nano-adsorbents for removal of methyl blue", *Int. J. Biol. Macromol.*, **50**, pp. 444–450 (2012).
13. Iqbal, M.J. and Ashiq, M.N. "Adsorption of dyes from aqueous solutions on activated charcoal", *Journal of Hazardous Materials.*, **B139**, pp. 57–66 (2007).
14. Zarezadeh-Mehrizi, M., Badiei, A., and Shahbazi, A. "Sulfonate-functionalized nanoporous silica spheres as adsorbent for methylene blue", *Research on Chemical Intermediates.*, **42**, pp. 3537–3551 (2016).
15. Senthilkumaar, S., Varadarajan, P.R., Porkodi, K., et al. "Adsorption of methylene blue onto jute fiber carbon: kinetics and equilibrium studies", *Journal of Colloid and Interface Science.*, **284**, pp. 78–82 (2005).
16. Ren, B., Xu, Y., Zhang, L., et al. "Carbon-doped graphitic carbon nitride as environment-benign adsorbent for methylene blue adsorption: Kinetics, isotherm and thermodynamics study", *Taiwan Institute of Chemical Engineers.*, **88**, pp. 114–120 (2018).
17. Belhachemi, M. and Addoun, F. "Comparative adsorption isotherms and modeling of methylene blue onto activated carbons", *Applied Water Science.*, **1**, pp. 111–117 (2011).
18. Fronczak, M., Demby, K., Strachowski, P., et al. "Graphitic carbon nitride doped with the s-block metals: Adsorbent for the removal of methyl blue and copper (II) ions", *ACS Paragon Plus Environment, Langmuir.*, **25**, pp. 7272–7283 (2018).
19. Peng, H., Lio, Z., and Tao, C. "Adsorption process of Vanadium (V) with melamine", *Water, Air, and Soil Pollution.*, **228**, p. 9 (2017).
20. Zhang, F., Zhao, Z., Tan, R., et al. "Removal of heavy metal ions from aqueous solution using Fe_3O_4-SiO_2-poly(1,2-diaminobenzene) core–shell sub-micron particles", *Journal of Colloid and Interface Science.*, **386**, pp. 205–212 (2012).
21. Rahimdokht, M. and Pajootan, E. "Titania/gum tragacanth nanohydrogel for methylene blue dye removal from textile wastewater using response surface methodology", *Polymer International.*, **68**, pp. 134–140 (2019).
22. Trinh, D.N., Viet, T.Q.Q., Nhu, T.H., et al. "Binary TiO_2/reduced graphene oxide nanocomposite for improving methylene blue photodegradation", *Vietnam Journal of Chemistry.*, **59**, pp. 395–404 (2021).
23. Saidi, F.Z. and Mokhtari, M. "Central composite design to optimize the degradation of methylene blue by fenton process", *Chemistry Select.*, **38**, pp. 11288–11293 (2019).
24. Zhao, T., Liu, R., Lu, J., et al. "Photocatalytic degradation of methylene blue solution by diphenylanthrazoline compounds", *Journal of Physical Organic.*, **30**, e3712 (2017).
25. Singh, A., Khare, P., Verma, S., et al. "Sunlight-induced selective photocatalytic degradation of methylene blue in bacterial culture by pollutant soot derived nontoxic graphene nanosheets", *ACS Sustainable Chem. Eng.*, **10**, pp. 8860–8869 (2017).
26. Ramar, V. and Balasubramanian, K. "Reduced graphene oxide/WO_3 nanorod composites for photocatalytic degradation of methylene blue under sunlight irradiation", *ACS Appl. Nano Mater.*, **5**, pp. 5512–5521 (2021).
27. Song, S., Wang, Y., Shen, H., et al. "Ultrasmall graphene oxide modified with Fe_3O_4 nanoparticles as a fenton-like agent for methylene blue degradation", *ACS Appl. Nano Mater.*, **11**, pp. 7074–7084 (2019).
28. Thakur, S., Das, P., and Mandal, S.K. "Solvent-induced diversification of CdS nanostructures for photocatalytic degradation of methylene blue", *ACS Appl. Nano Mater.*, **6**, pp. 5645–5655 (2020).
29. Bantawal, H. "Porous graphene wrapped $SrTiO_3$ nanocomposite: Sr-C bond as an effective coadjutant for high performance photocatalytic degradation of methylene blue", *ACS Appl. Nano Mater.*, **10**, pp. 6629–6636 (2019).
30. Chen, X., Liu, L., Yu, P.Y., et al. "Increasing solar absorption for photocatalysis with black hydrogenated titanium dioxide nanocrystals", *Science.*, **331**, pp. 746–750 (2011).

31. Choi, J.U., Kim, Y.G., and Jo, W.K. "Multiple photocatalytic applications of non-precious Cu-loaded g-C_3N_4/hydrogenated black TiO_2 nanofiber heterostructure", *Applied Surface Science.*, **473**, pp. 761–769 (2019).
32. Li, Y., Fu, R., Gao, M., et al. "B–N co-doped black TiO_2 synthesized via magnesiothermic reduction for enhanced photocatalytic hydrogen production", *International Journal of Hydrogen Energy.*, **44**, pp. 28629–28637 (2019).
33. Ren, L., Zhou, W., Sun, B., et al. "Defects-engineering of magnetic γ-Fe_2O_3 ultrathin nanosheets/mesoporous black TiO_2 hollow sphere heterojunctions for efficient charge separation and the solar-driven photocatalytic mechanism of tetracycline degradation", *Applied Catalysis B: Environmental.*, **240**, pp. 319–328 (2019).
34. Shoja, A., Habibi-Yangjeh, A., Mousavi, M., et al. "Preparation of novel ternary TiO_2 QDs/CDs/AgI nanocomposites with superior visible-light induced photocatalytic activity", *Journal of Photochemistry and Photobiology A: Chemistry*, **385**, 112070 (2019).
35. Khaled, A., Nemr, A.E., El-Sikaily, A., et al. "Removal of Direct N Blue-106 from artificial textile dye effluent using activated carbon from orange peel: Adsorption isotherm and kinetic studies", *Journal of Hazardous Materials*, **165**, pp. 100–110 (2009).
36. Langmuir, I. "The constituation and fundamental proprties of solids and liquids, Part I. solids", *Journal of American Chemical Society.*, **38**, pp. 2221–2295 (1916).
37. Freundlich, H. "Over the Adsorption in Solution", *J. Phys. Chem.*, **57**, pp. 385–471 (1906).
38. Crini, G., Peindy, H.N., Gimbert, F., et al. "Removal of C.I. basic green 4 (Malachite green) from aqueous solutions by adsorption using cyclodextrin-based adsorbent: Kinetic and equilibrium studies", *Sep. Purif. Technol.*, **53**, pp. 97–110 (2007).
39. Senthilkumaar, S., Varadarajan, P.R., Porkodi, K., et al. "Adsorption of methylene blue onto jute fiber carbon: kinetics and equilibrium studies", *Journal of Colloid and Interface Science.* **284**, pp. 78–82 (2005).
40. Ren, B., Xu, Y., Zhang, L., et al. "Carbon-doped graphitic carbon nitride as environment-benign adsorbent for methylene blue adsorption: Kinetics, isotherm and thermodynamics study", *Journal of the Taiwan Institute of Chemical Engineers.*, **88**, pp. 114–120 (2018).
41. Han, R. and Zhang, J. "Study of equilibrium, kinetic and thermodynamic parameters about methylene blue adsorption onto natural zeolite", *Chemical Engineering Journal.*, **145**, pp. 496–504 (2009).
42. Xie, J. and Li, C.J. "Chitosan modified zeolite as a versatile adsorbent for the removal of different pollutants from water", *Fuel.*, **103**, pp. 480–485 (2013).
43. Basava, V. and Rao, M. "Adsorption studies on treatment of textile dyeing industrial effluent by flyash", *Chemical Engineering Journal.*, **116**, pp. 77–84 (2006).
44. Djilani, C. and Zaghdoudi, R. "Adsorption of dyes on activated carbon prepared from apricot stones and commercial activated carbon", *Journal of the Taiwan Institute of Chemical Engineers.*, **53**, pp. 112–121 (2015).
45. Senthilkumaar, S., Varadarajan, P.R., Porkodi, K., et al. "Adsorption of methylene blue onto jute fiber carbon: kinetics and equilibrium studies", *Journal of Colloid and Interface Science.*, **284**, pp. 78–82 (2005).
46. Fu, L., Zhang, L., Wang, S., et al. "Silica Nanoparticles Modified with Trithiocyanuric Acid as a Potential Adsorbent for Removal of Ag+ from Aqueous Solutions", *Water, Air, & Soil Pollution.*, **228**, p. 9 (2017).
47. Han, R., Wang, Y., Yu, W., et al. "Biosorption of methylene blue from aqueous solution by rice husk in a fixed-bed column", *Journal of Hazardous Materials.*, **141**, pp. 713–718 (2007).
48. Fernandes, A.N., Almedia, C.A.P., Menezes, C.T.B., et al. "Removal of methylene blue from aqueous solution by peat", *Journal of Hazardous Materials.*, **144**, pp. 412–419 (2007).
49. Dong, Y., Lu, B., Zang, S., et al. "Removal of methylene blue from coloured effluents by adsorption onto SBA-15", *Journal of Chemical Technology and Biotechnology.*, **86**, pp. 616–619 (2011).
50. Zhao, M. and Liu, P. "Adsorption behavior of methylene blue on halloysite nanotubes", *Microporous and Mesoporous Materials.*, **112**, pp. 419–424 (2008).
51. McKay, G. "The adsorption of dyestuffs from aqueous solution using activated carbon. analytical solution for batch adsorption based on external mass transfer and pore diffusion", *Chemical Engineering Journal.*, **27**, pp. 187–196 (1983).
52. Ausavasukhi, A., Kampoosaen, C., and Kengnok, O. "Adsorption characteristics of Congo red on carbonized leonardite", *Journal of Cleaner Production.*, **134**, pp. 506–514 (2016).

Biographies

Meisam Soleimani was born in 1982 in Shiraz. He completed his undergraduate studies at Chemistry and Chemical Engineering Institute of Iran, Tehran in 2009. In 2018, he was awarded PhD from University of Münster (Germany) in the field of Ga-N Lewis Pairs. He is currently a postdoctoral researcher at University of Tehran in the field of nano-inorganic chemistry.

Elham Boorboor Azimi received her doctorate under the supervision of Professor Badiei from University of Tehran. Her research interests are inorganic nanomaterials and photocatalysts.

Mitra Mousavi received her PhD degree from Mohaghegh Ardebili University in Physical Chemistry. She is currently a Postdoctoral researcher at the

University of Tehran in the fields of Photocatalysis, Electrochemistry and Chemometrics.

Jahan Bakhsh Ghasemi received his PhD degree from University of Shiraz in Analytical Chemistry in 1995 with research on thermodynamic and kinetic of complexation. He became a Professor at the Department of Chemistry, The University of Tehran. He was a visiting researcher at University of Delaware in 2006 with study on signal denoising algorithms. His research interests cover chemometrics, medicinal chemistry, thermodynamics, and kinetics study of protein-ligands and host-guest interactions, software applications for refinement of analytical data, interfacing, and automation and application of various multivariate techniques in nanotechnology and photocatalysts, and food technology.

Alireza Badiei received his doctorate under the supervision of Professor Laurent Bonneviot from Laval University, Canada, in 2000. He started a research career at University of Tehran in 2000. His research interests cover inorganic nanomaterials and applications in photocatalysts, optical sensors, and green chemistry.